Disk-averaged Spectra & Light-curves for Terrestrial Planets

G. Tinetti (NAI-NRC/Caltech), V. S. Meadows (Caltech), D. Crisp (JPL),
W. Fong (Caltech), T. Velusamy (JPL), E. Fishbein (JPL), M. Allen (JPL)

Abstract

NASA and ESA are currently studying mission concepts for space-based observatories to search for and characterize extrasolar terrestrial planets. Any planet directly detected by this first generation of space- missions will be resolved only as point sources. Basic information can be gleaned from the object's distance from the star and its apparent brightness, but the presence of a planetary atmosphere of unknown composition will complicate the determination of planetary properties. Disk- averaged spectroscopy will be our best tool for discriminating between Jovian and Terrestrial planets, and between Terrestrial planets of different types. Spectrally-dependent light-curves and disk-averaged spectra of a plausible range of extrasolar terrestrial planets can be simulated to determine the detectability of biosignatures by proposed space- based observatories.

Introduction

The principal goal of the NASA TPF and ESA Darwin mission concepts is to detect and characterize extrasolar terrestrial planets. TPF-C, TPF-I and Darwin are expected to survey nearby stars and directly detect planetary systems that include terrestrial-sized planets in their habitable zones.

We present here the first simulations of disk-averaged spectra and light curves of Mars [Ref. 8] (a good example of a likely abiotic planet) and Earth (the only example of life supporting planet known, so far...). This work helped us to understand how to retrieve information from disk- averaged spectra, and how to possibly detect biosignatures from remote sensing observations. The core of the model is a spectrum-resolving (line-by-line) atmospheric/surface radiative transfer model (SMART) developed by David Crisp [Ref. 2, 3]. Martian surface albedos and atmospheric properties from General Circulation Models have been used as input for Mars. AIRS (Atmospheric Infrared Sounder) data were used as input for Earth [Ref.7] (fig. 1).

These experimental data have been processed and mapped on the sphere using a pixelization scheme created for Planck and WMAP missions (Healpix) [Ref.4] (fig. 2). For each of the pixels SMART was run to generate a database of synthetic spectra for a variety of viewing angles, illuminations, surface type and cloud coverage. Finally, a model was created in which the user specifies spatial resolution and observing

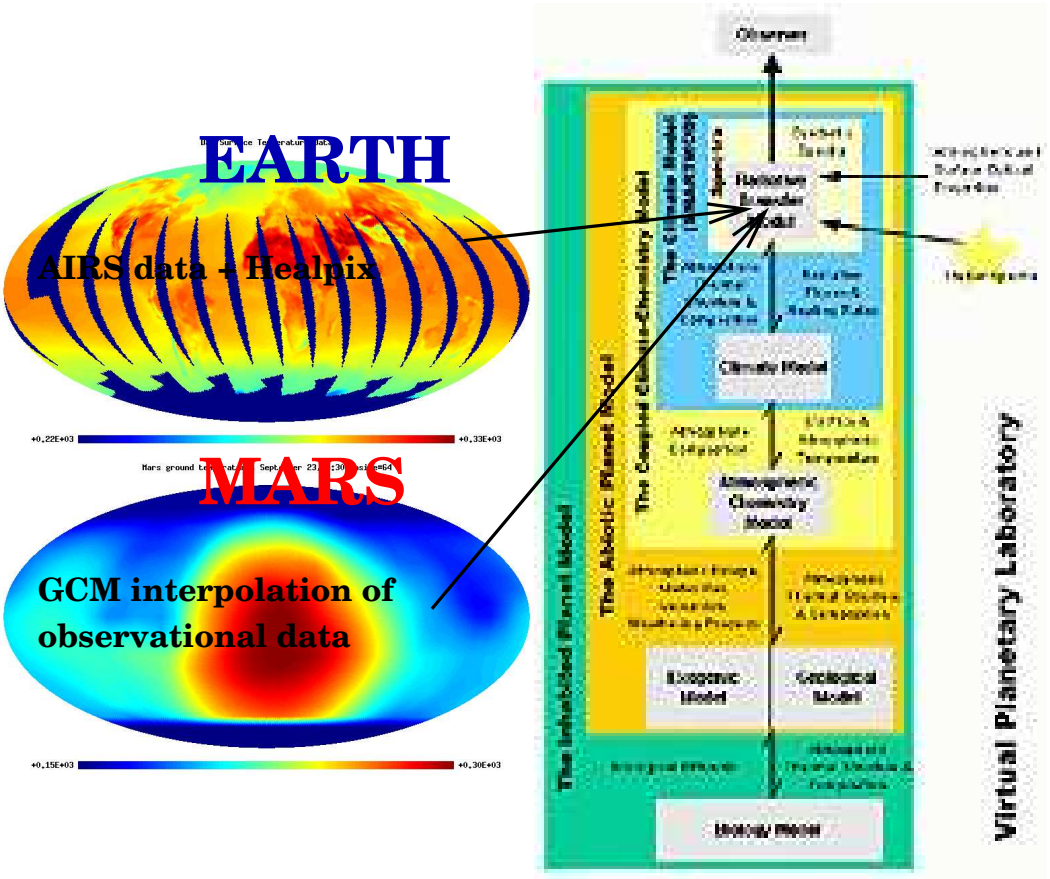

Figure 1: *We have included in our simulation 6 different surface types for Earth: Ocean, Ice, Tundra, Forest, Grass, Ground and 3 cloud types: cirrus, strato-cumulus, alto-stratus. We have used Atmospheric InfraRed Sounder data as input for SMART (Spectral Mapping Atmospheric Radiative Transfer Model, by D. Crisp).*
For Mars we have used GCM interpolation of atmospheric/surface observational data as input to SMART, and two surface types: basalt and ice/dirty ice [ref. 8].

position, and the program selects the appropriate synthetic spectra generated by SMART and creates the final view, which can then be averaged on the disk [Ref. 8].

These results have been processed with an instrument simulator to improve our understanding of the detectable characteristics as viewed by the first generation extrasolar terrestrial planet detection and characterization missions (by T. Velusamy) fig. 12, 13, 14, 15 [Ref. 5, 6].

The Earth-model has been validated against disk-averaged observations of the Earth by the Mars Global Surveyor Thermal Emission Spectrometer (MGS TES) fig. 10 [Ref. 1] and Earth-shine spectra [Ref. 12] and the Mars-model has been validated against spectra recorded by Mariner 9 Interferometer Spectrometer (IRIS) fig. 11 [Ref. 11, 8]. The model generates a variety of products including globally averaged synthetic spectra, light-curves and the spectral variability at visible and IR wavelengths as a function of viewing angle. These tools have been used for simulations of an increasingly frozen Mars (fig. 7), an increasingly cloudy/forested/oceanic

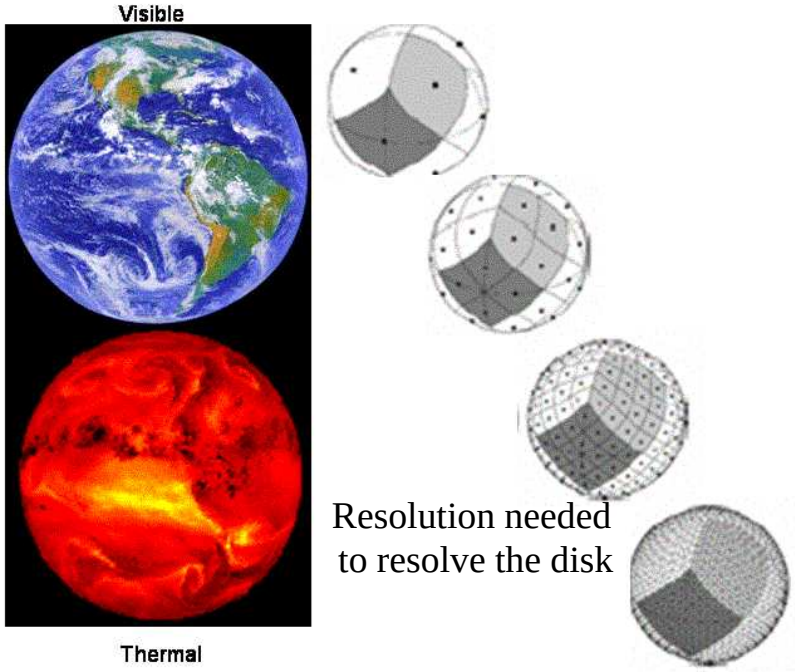

Figure 2: *Disk-averaged solar and IR spectra of the Earth and Mars were generated from several vantage points (ie over the pole, over the equator, etc.) to assess the effects of illumination, clouds and surface albedos on the spectral information content. For both model we have used a resolution of 48 pixels for the atmosphere and 3,072 pixels for the surface (Healpix pixelization of the sphere, ref. 4).*

Earth (fig. 6, 5), and analyzed to determine the detectability of biosignatures on an Earth-like planet (e.g. red-edge signal, fig. 9).

1 Disk-averaged synthetic spectra of Earth and Mars. IR and visible

Disk-averaged solar and IR spectra of Earth and Mars were generated from several vantage points (ie over the pole, over the equator, etc.) to assess the effects of illumination (the sun position is kept fixed, the observer position -and correspondingly the illumination- changes) and surface albedos on the spectral information content. For both Earth and Mars the visible spectra show large variations in intensity as a function of planetary phase. Similarly, large variations in overall intensity are seen for the MIR spectra for Mars, driven by the difference in day-night surface temperatures on Mars, and the resulting disk-averaged temperature seen by the observer. This variability in Martian surface temperature is relatively high for a terrestrial planet with an atmosphere, as Mars lacks an ocean, and its atmosphere is thin, so it has a very limited heat capacity to buffer its climate and even out day/night variations.

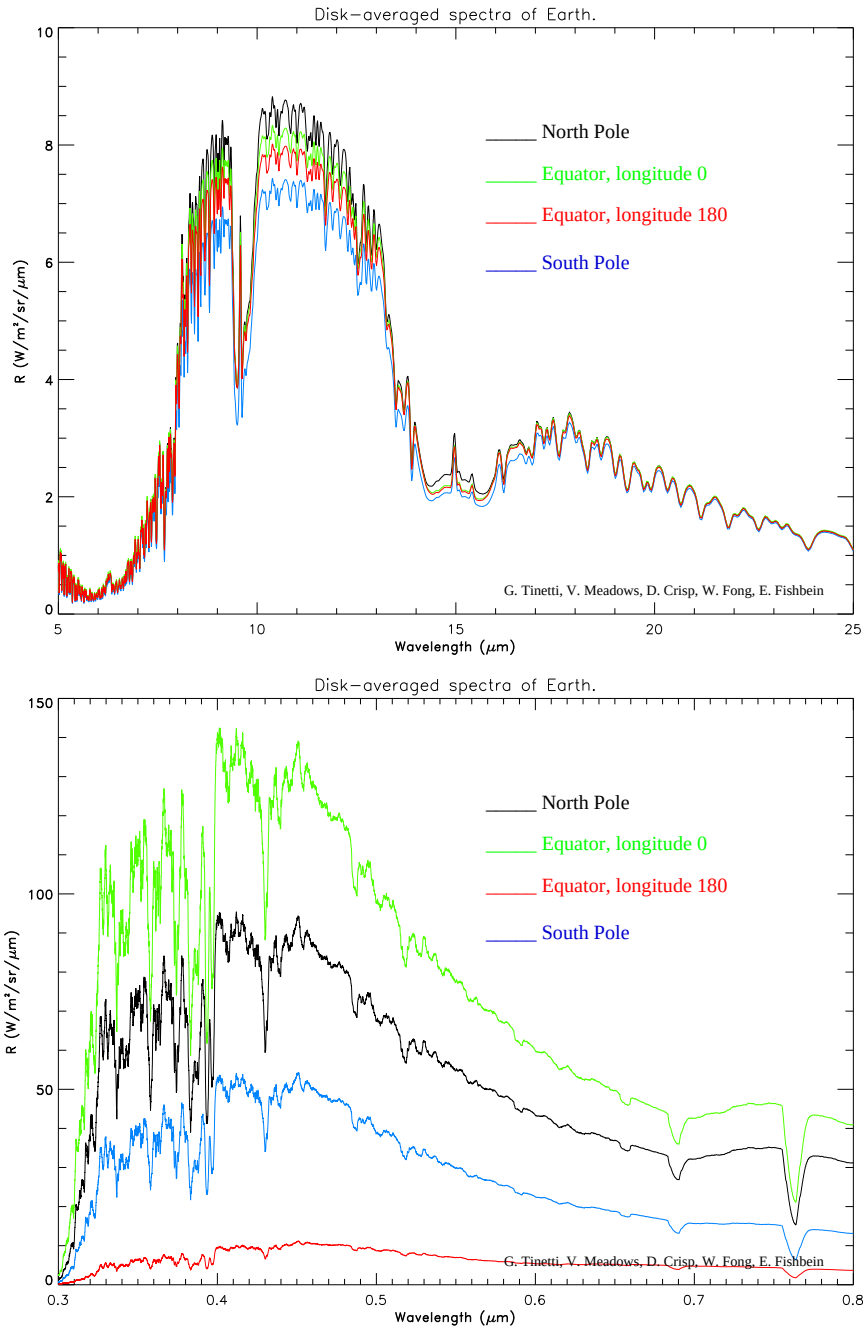

Figure 3: *Earth solar (fig. at the bottom) and IR disk-averaged spectra. We have included in this simulation 6 different surface types: Ocean, Ice, Tundra, Forest, Grass, Ground. There are no clouds. We have used AIRS data as input for SMART (Spectral Mapping Atmospheric Radiative Transfer Model, by D. Crisp). We have used a resolution of 48 pixels for the atmosphere and 3,072 pixels for the surface. Sun position: latitude= 20.77°, longitude 1.65° (corresponding to July 20th 2002, 0 p. m. UT). Viewing position: black curve, North Pole; light blue curve, South Pole; green curve, Equator-longitude 0°, red curve, equator-longitude 180°.*

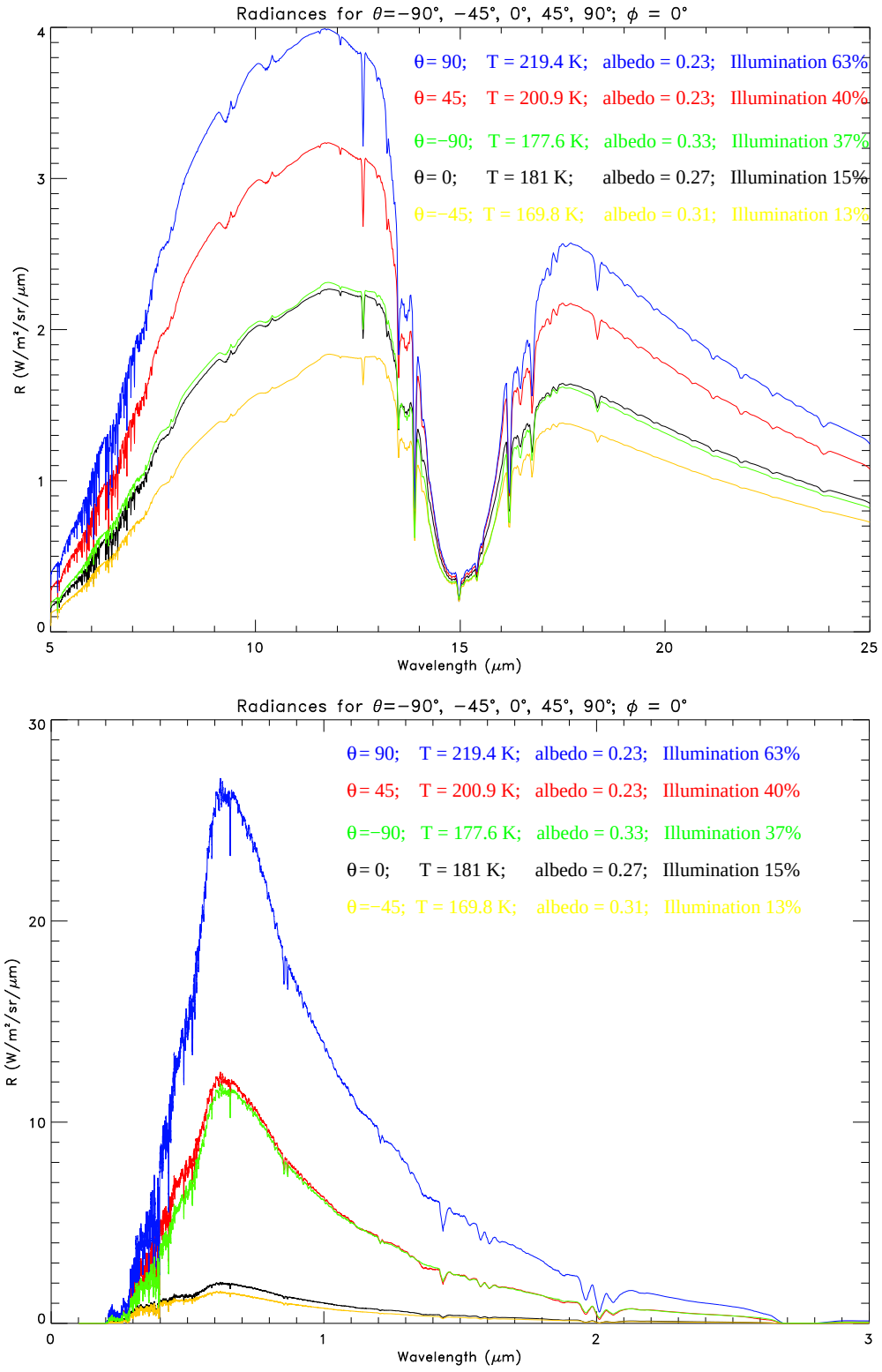

Figure 4: *Variability of disk-averaged synthetic spectra [Ref. 8]. Synthetic spectra for sub-viewer points with different latitudes (longitude, $\phi = 0°$): $\theta = 0°$, $\theta = 45°$, $\theta = 90°$, $\theta = -45°$, $\theta = -90°$ for a day corresponding to $L_s = 104.6$. The disk-averaged surface temperature, solar albedo and illumination are indicated as well.*
The polar caps extend $\sim 15°$ to the South in the northern hemisphere, and $\sim 40°$ to the North in the southern hemisphere. The sun position derived from the JPL Horizons Ephemeris System is 24.63° latitude, and 169.99 ° longitude.

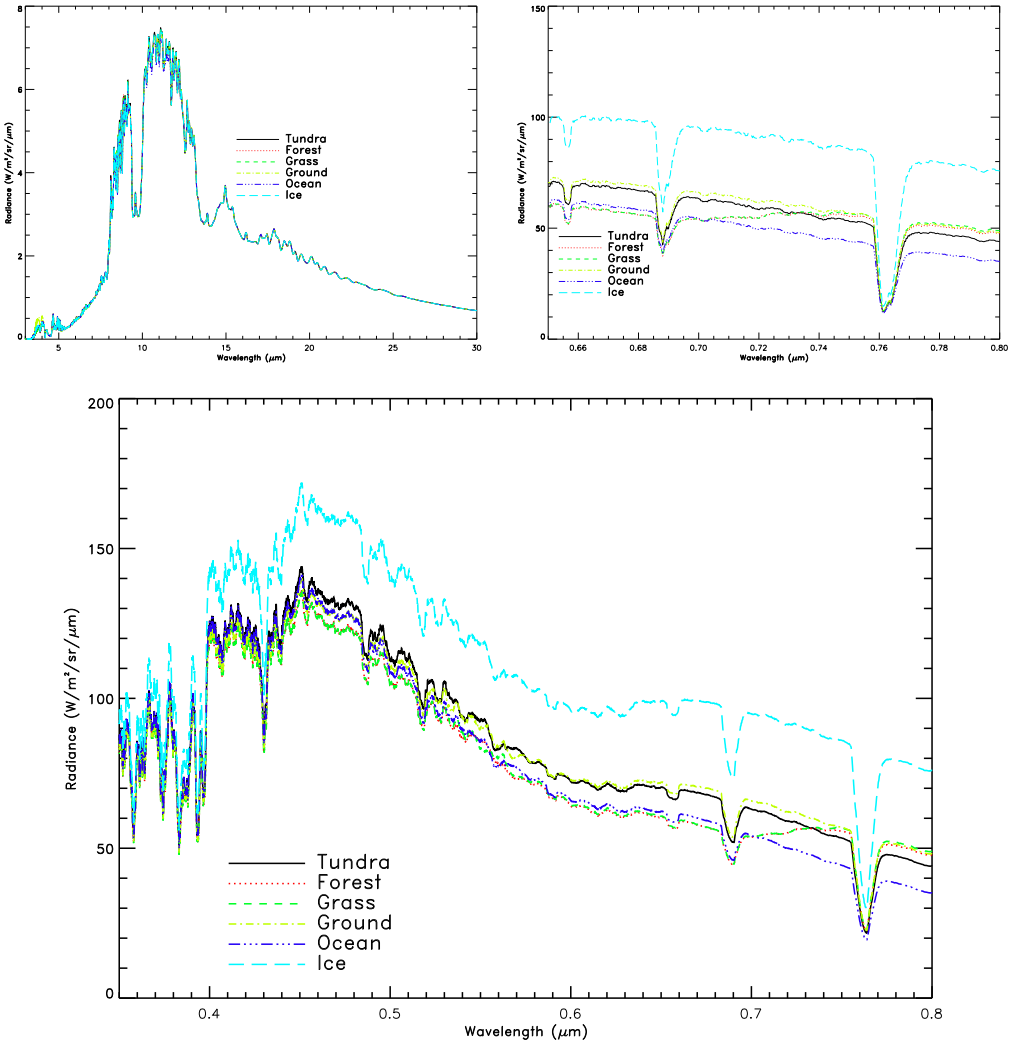

Figure 5: *Spectra of various surface types. Almost no differentiation in the IR. In the visible on the contrary we have pronounced differences in the spectra. In the band 0.7-0.8 μm we can recognize very clearly the red-edge (leafy plants reflect sunlight strongly in this band, fig. 9).*

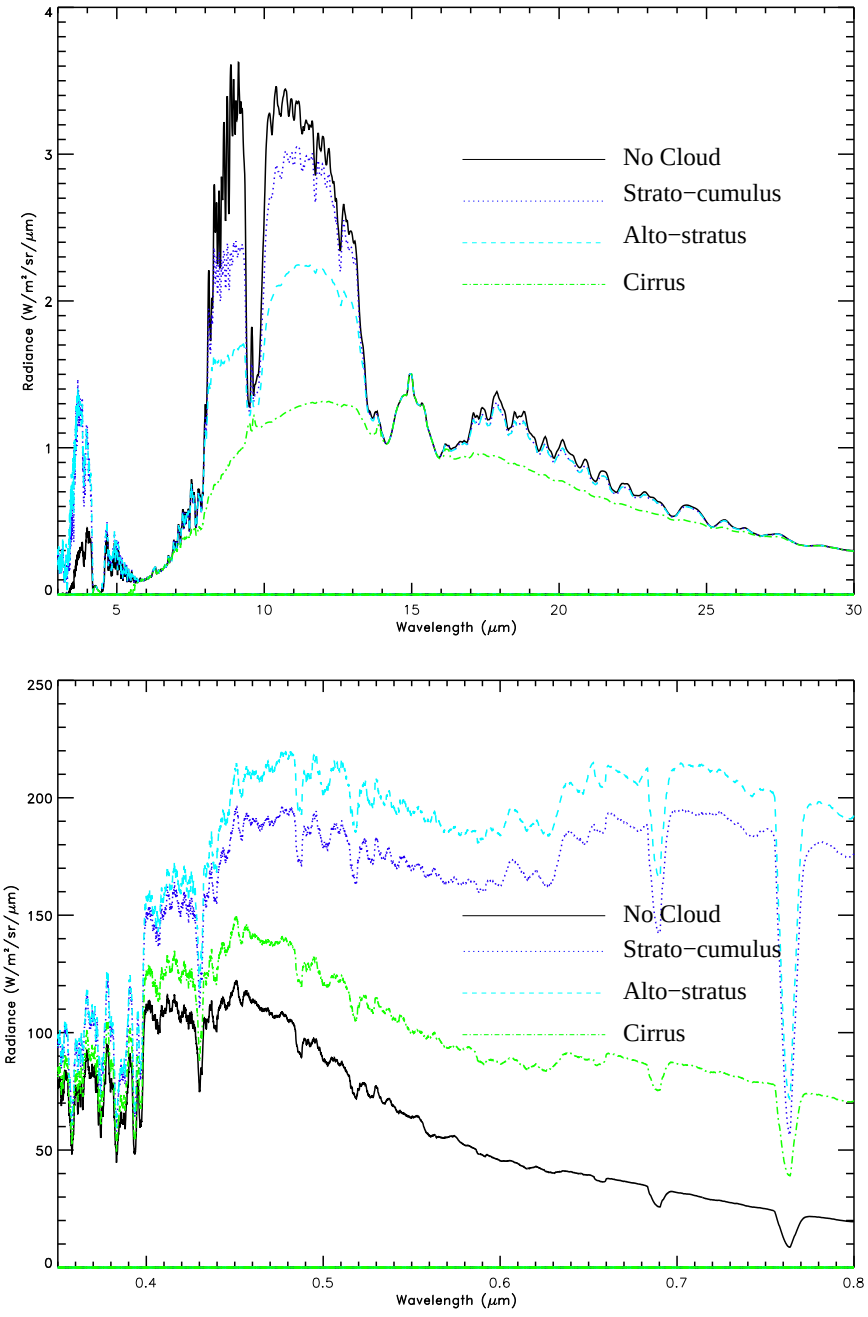

Figure 6: *Spectra of different cloud types. The contribution of clouds is dramatic. We have to include them in order to have a realistic model (see fig. 10). Even with clouds, the most important features are still detectable in the IR. In the visible it is more difficult (fig. 9).*

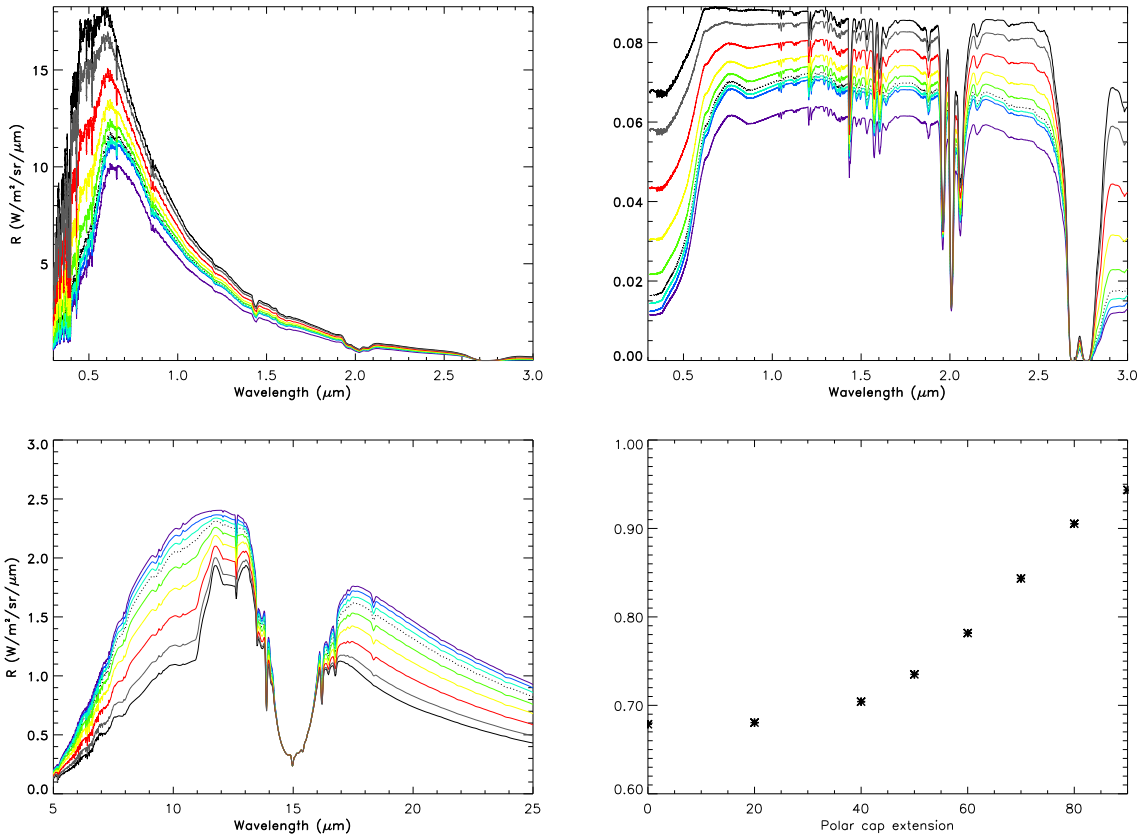

Figure 7: *Disk-averaged spectra of the southern polar-cap area (supposed extending for* 0° *(violet curve),* 20° *(dark-blue curve),* 30° *(light-blue curve),* 40° *(dotted curve),* 50° *(green curve),* 60° *(yellow curve),* 70° *(red curve),* 80° *(grey curve),* 90° *(black curve) For increasing extension of the polar-cap area the* CO_2 *ice features are more and more detectable. The figures on the top, show the UV-nearIR part of the spectrum: radiation intensity is given in* $W/m^2/sr/\mu$ *in the fig. on the left, and divided by the total solar flux at the top of the atmosphere in the one on the right.*
On the bottom is shown on the left the IR part of the spectrum. The quantities plotted in the fig. on the right are $\frac{\int_{\lambda_1}^{\lambda_2} \mathcal{I}\, d\lambda}{\int_{\lambda_3}^{\lambda_4} \mathcal{I}\, d\lambda}$*, where* $\mathcal{I}(\lambda)$ *are the disk-averaged radiation intensities corresponding to different extensions of the polar-cap area. For this figure we have chosen* $\lambda_1 = 0.5$*,* $\lambda_2 = 0.7$*,* $\lambda_3 = 0.7$ *and* $\lambda_4 = 0.9$

3 Light curves and detectability of biosignatures

Time dependent variations in the disk-averaged spectra, or "light curve" can provide additional information about spatial variations.

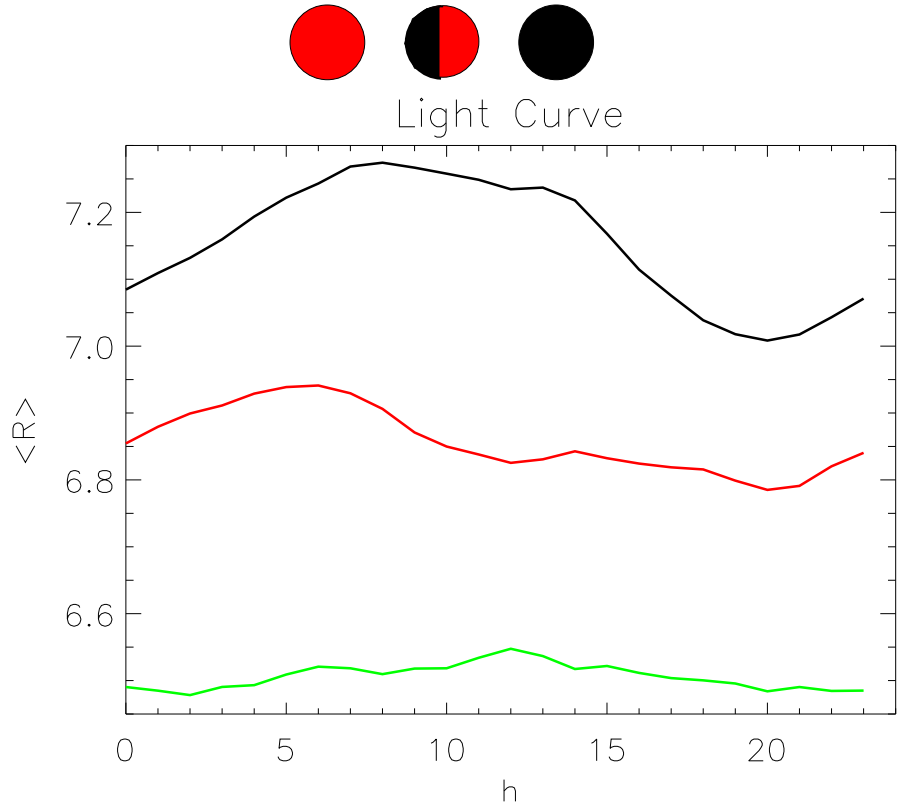

Figure 8: *Light-curves following the diurnal rotation of the planet for the intervals 8-13 μm for the IR.*
The quantity plotted is $\frac{\int_{\lambda_1}^{\lambda_2} \mathcal{I}\, d\lambda}{\int_{\lambda_1}^{\lambda_2} d\lambda}$, *where* $\mathcal{I}(\lambda)$ *is the disk-averaged radiation,* λ_1 *and* λ_2 *are the extremes of the chosen interval. The phases considered are totally illuminated (black-line), totally dark (green-line) and dichotomies (red-line).*

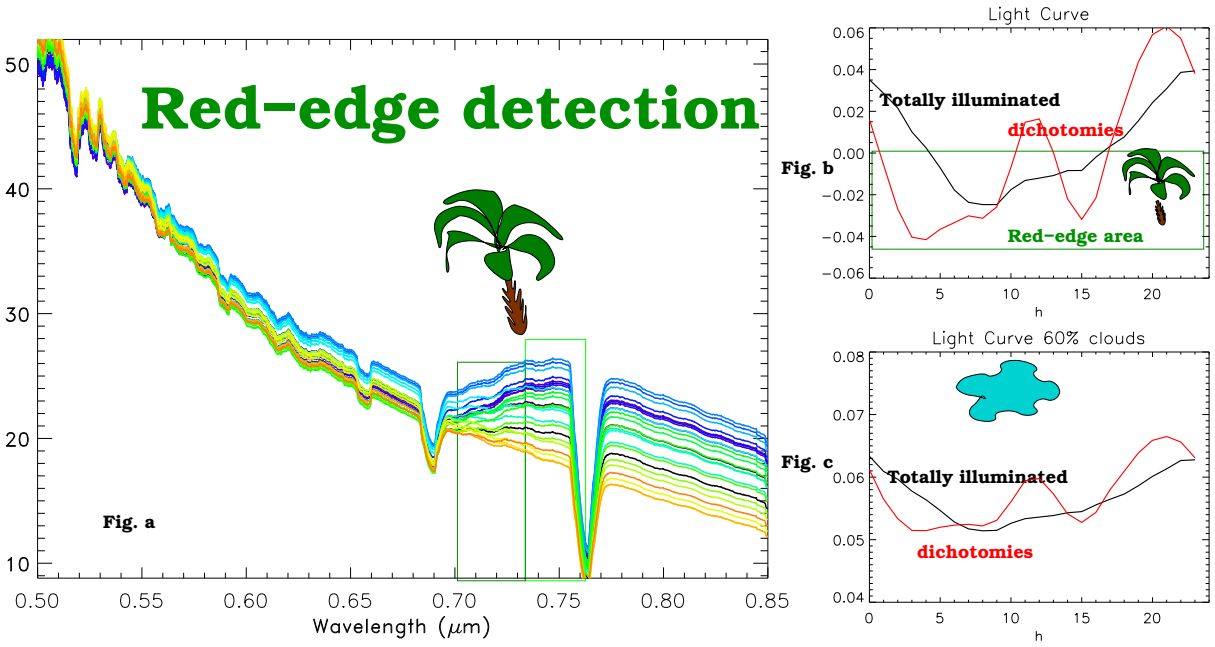

Figure 9: *Light-curves following the diurnal rotation of the planet to detect the red-edge effect (fig. b). The quantity plotted is* $\frac{\int_{0.7}^{0.73} \mathcal{I}\, d\lambda - \int_{0.73}^{0.76} \mathcal{I}\, d\lambda}{\int_{0.5}^{0.7} d\lambda}$*, where* $\mathcal{I}(\lambda)$ *is the disk-averaged radiation intensity calculated from different vantage points in phase with the sun diurnal path(fig. a). When this expression is negative it means that we can detect the red-edge. The phases considered are totally illuminated, and dichotomies.*
When we add 60% cloud coverage (fig. c) the signal becomes positive (see fig. 2): in this case the clouds are uniformely distributed, so we still detect the shape of fig. b, but as soon as we consider randomly distributed clouds, the red-edge signal is hardly detectable.

4 Earth: Validation with observed spectra

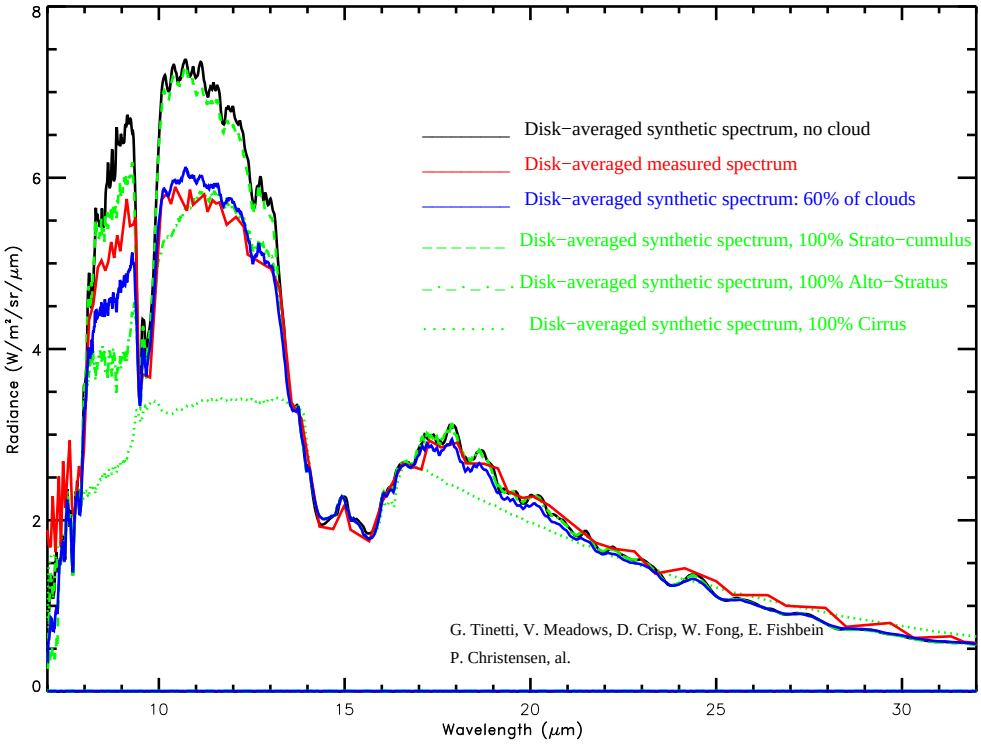

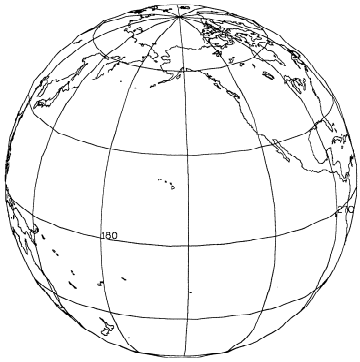

Figure 1. View of the Earth at 1730 UT on November 24, 1996, from the Mars Global Surveyor at the midpoint of the TES Earth observations.

Figure 10: *Fig. on top: Disk-averaged spectrum of Earth observed by Mars Thermal Emission Spectrometer (TES) (red) [Ref. 1] compared with the synthetic one produced in almost the same conditions with 60% of clouds (blue) and without clouds (black). Plots in green show the contribution of different cloud-types. Fig. at the bottom: we show the view of the Earth at 17:30 UT on November 24, 1996, from the MGS [Ref. 1].*

Mars: validation with observed spectra

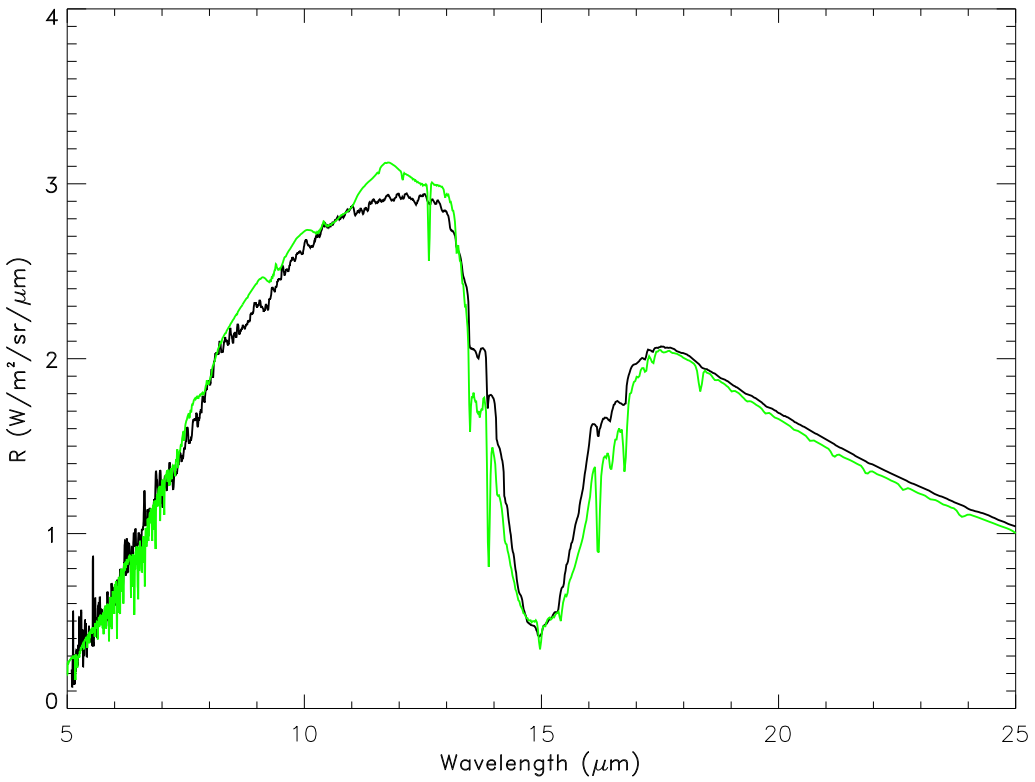

Figure 11: *Disk-averaged IR spectrum of Mars observed by IRIS-Mariner 9 in July 1972 (black line, after [Ref. 11]). The sub-observer point is in the mid-latitudes, and the atmosphere was relatively free of dust when the data spectrum was taken. For comparison, we show one of our simulated spectra (green line).*
The discrepancies in the 13-17μm band are certainly due to a slightly different atmospheric temperature profile, a better agreement with the data could be achieved using specific algorithms to retrieve the temperature distribution from the observed spectrum. Moreover, in the Mariner 9 spectrum there is still a small quantity of dust, absorbing in the 8-13μm band; our synthetic spectrum is dust-free. Finally, since the synthetic spectrum has a higher resolution, some absorption features are more visible.

5 Simulation of a TPF detection of a Earth-like and Mars-like planet

Our synthetic disk-averaged spectra were run through a TPF observation system simulator for different spectral resolutions. The TPF book design has been assumed for these calculations and the planet was placed around a G star that is 10pc distant. TPF will provide only disk-averaged spectra with possible spectral resolutions of ~75 (visible) and ~25 (MIR), depending on final architecture [Ref. 5,6].

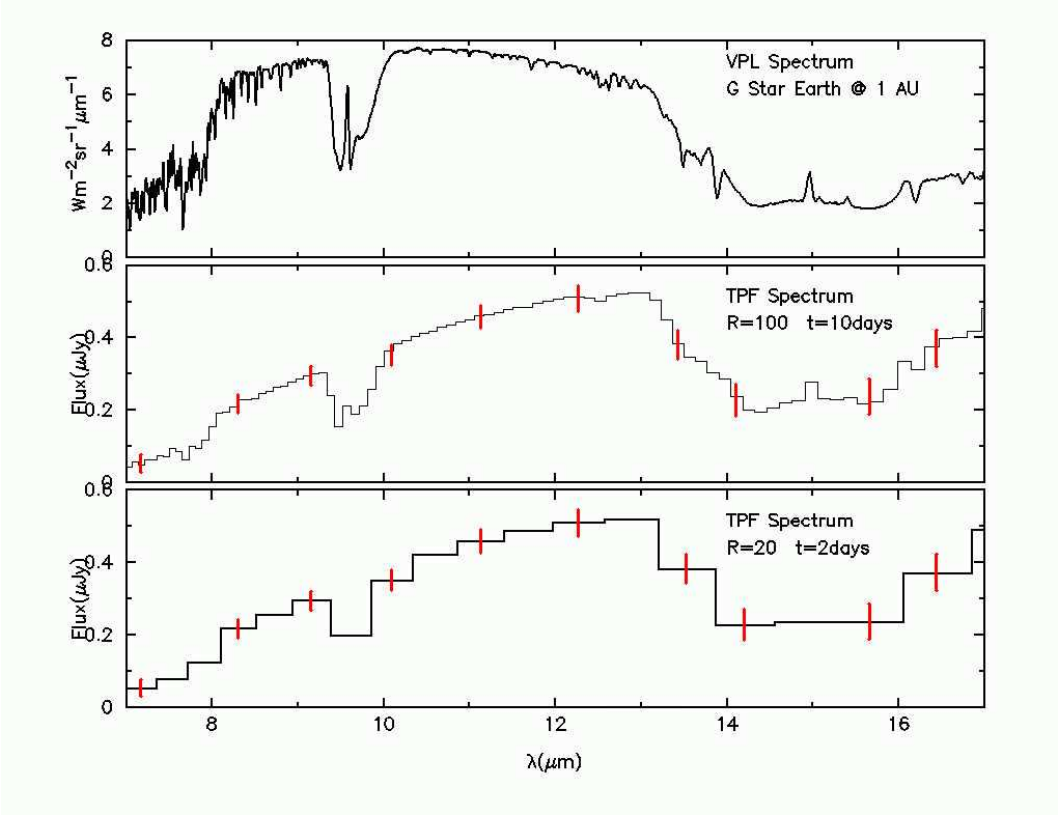

Figure 12: *Simulation of TPF-Interferometer detection of a Earth-like planet orbiting around a G star. The top spectrum in each set is at high-resolution, and the middle and lower panels show R~100 (at 10 days integration) and R~20 (at 2 days integration) respectively. 1-σ error bars are shown in red. We recall that the wavelength range currently proposed and desirable should be 6.-17 microns for the interferometer, with spectral resolution of 25-50.*

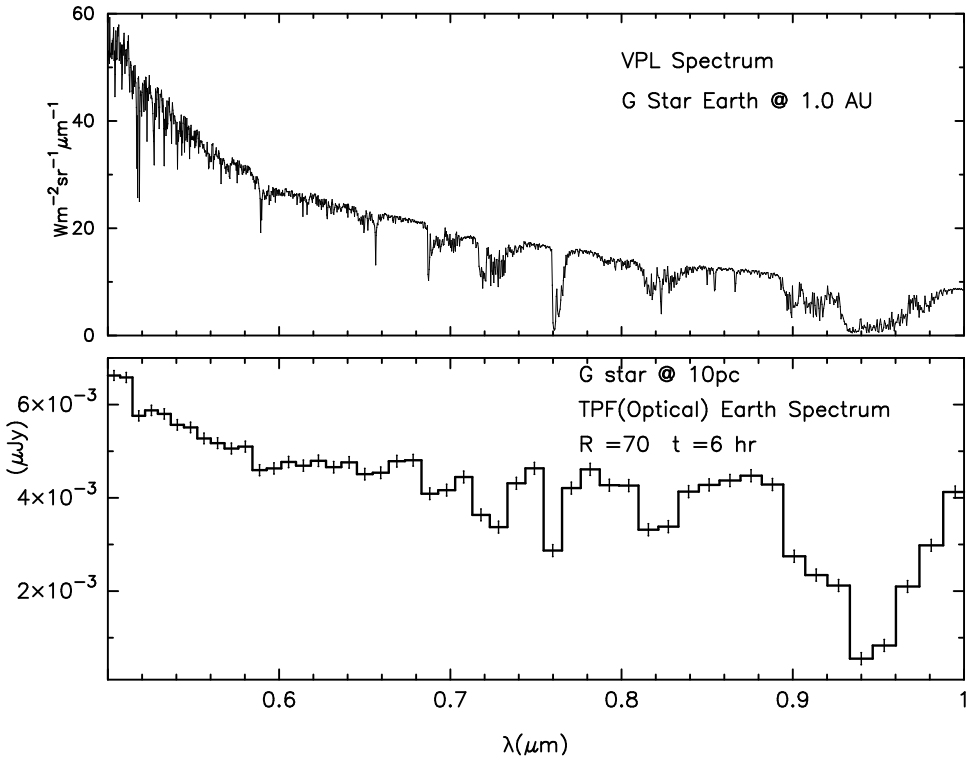

Figure 13: *Simulation of TPF-Coronograph detection of a Earth-like planet orbiting around a G star. These plots have been produced by processing the synthetic spectra with an observational system simulator of the TPF coronograph, at spectral resolutions R= 70 with corresponding integration time of 6h. The error bars in the spectra represent rms noise (1 sigma) in the TPF measurement in each spectral channel for the integration.*

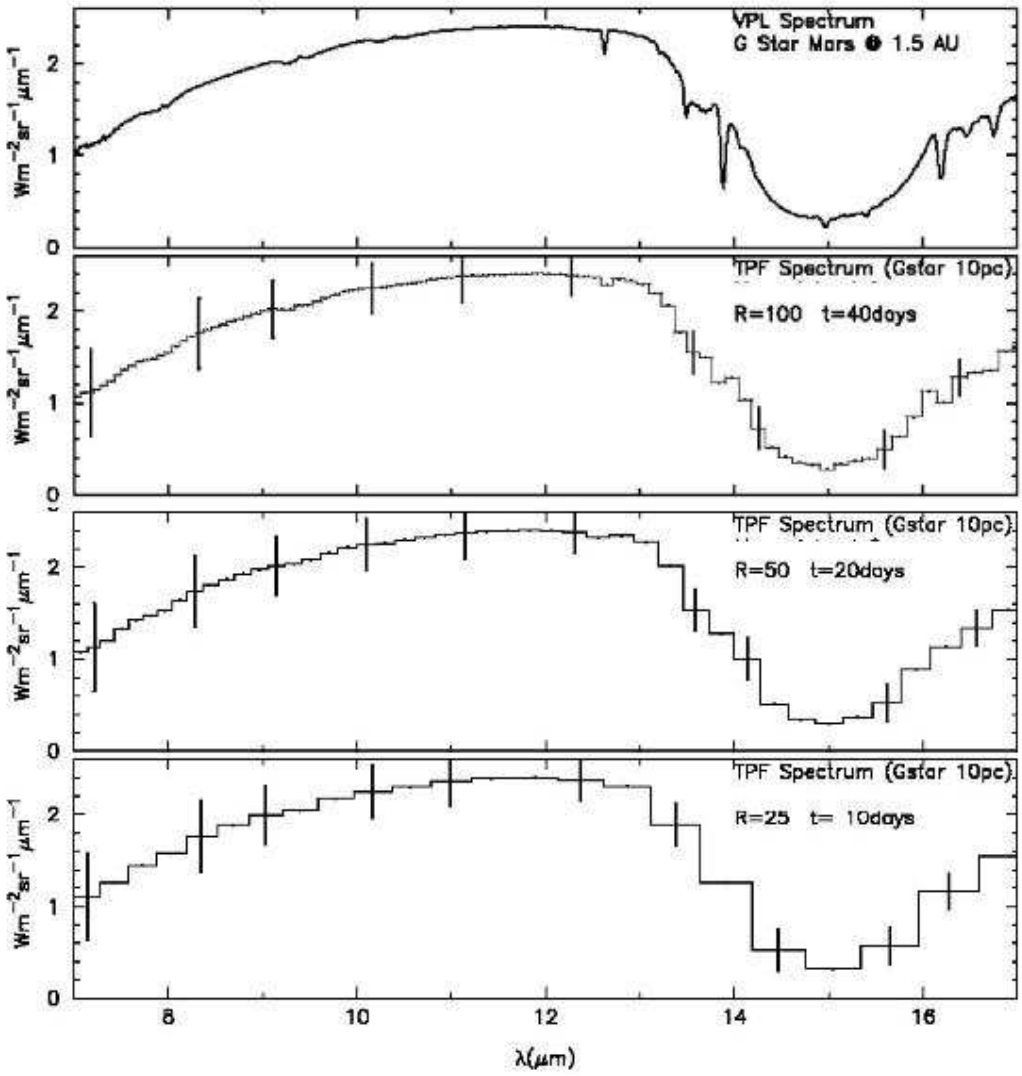

Figure 14: *Simulation of TPF detection of a disk averaged spectrum of a basalt-Mars (distance: 10 pc) at MIR wavelengths. The three panels show the interferometer instrument simulator results for increasing degradation in the spectral resolving power, R ($\lambda/\Delta\lambda$) = 100, 50 and 25. [Ref. 8].*

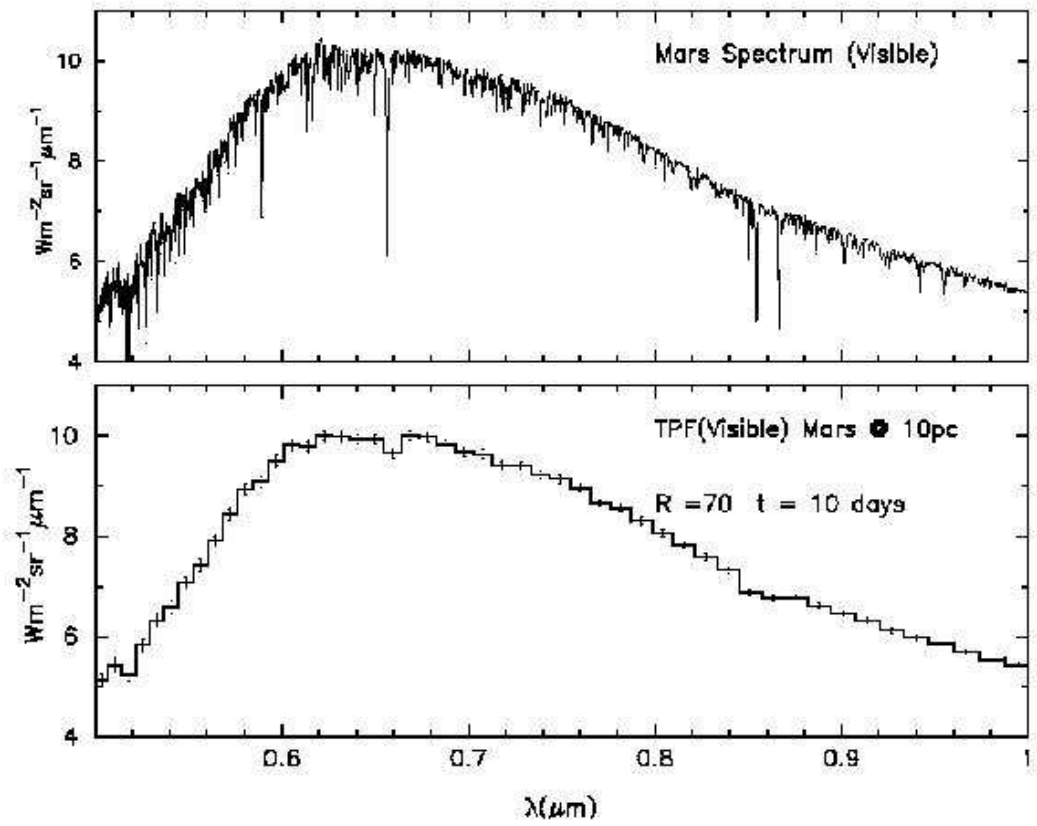

Figure 15: *Simulation of TPF detection of a disk averaged spectrum of a basalt-Mars (distance: 10 pc) at VIS wavelengths. The lower panel shows the coronograph instrument simulator result at a spectral resolving power of R= 70. Most of the absorption lines are due to the star-spectrum [Ref. 8].*

6 Self-consistent exo-atmospheres and different orbital geometries for extrasolar terrestrial planets: "being prepared for the unexpected".

In the previous sections we have presented the simulation of planets belonging to our solar system (or ones very similar to them) to validate the methods. Extrasolar terrestrial planets might have a wider range of atmospheric chemical composition (fig. 17), orbital distances, eccentricities, and obliquities than those found in our solar system [Ref. 9, 10]. The NASA-TPF and ESA-Darwin are missions of exploration: "being prepared for the unexpected" -quoting A. Léger- is mandatory.

To simulate a wider range of terrestrial planets than those found in our system we have coupled a versatile climate model (G. Tinetti and D. Crisp, H. Savijarvi, H. Inada) with a chemistry model, Kinetics (developed by M. Allen and Y. Yung at Caltech). The surface/atmosphere radiative transfer model SMART (D. Crisp), will then be used to generate time-dependent spectra of these environments throughout the annual cycle.

clim_spectra

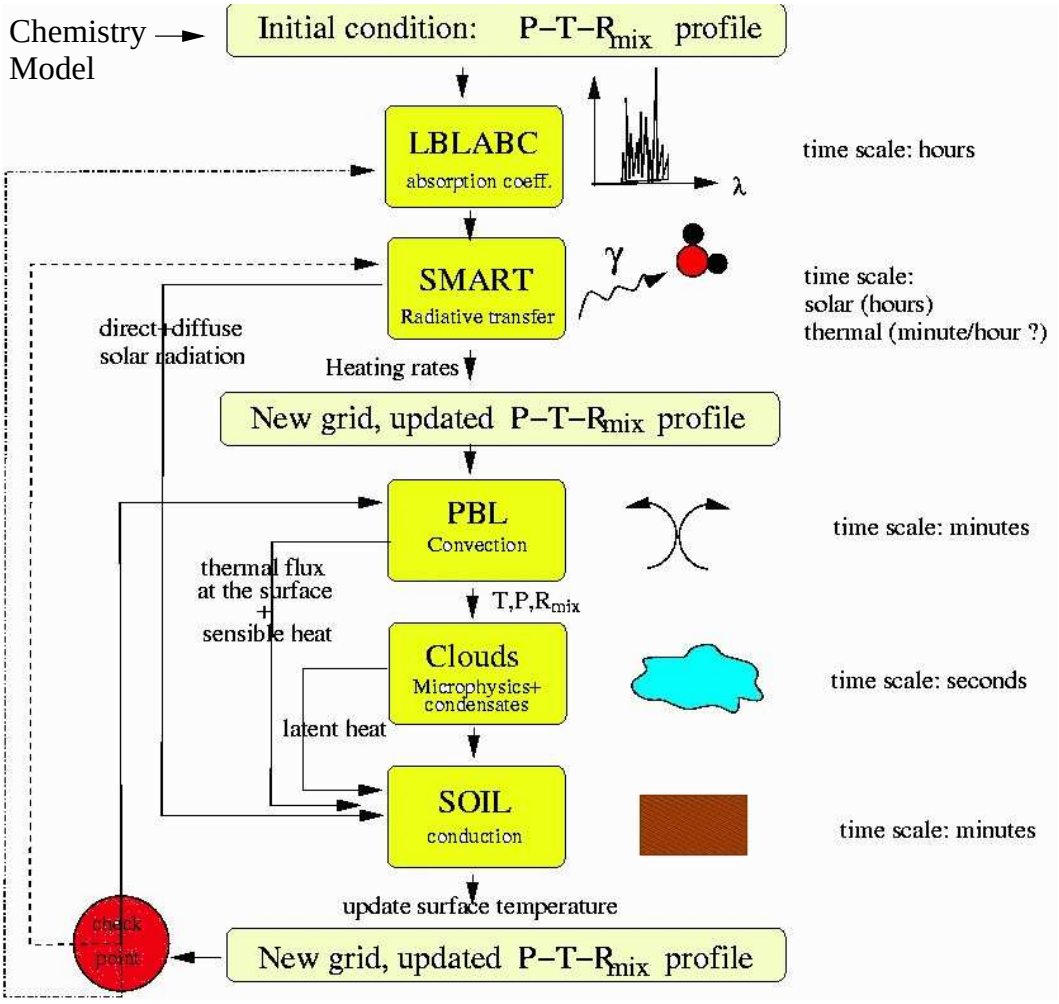

Earth on an eccentric orbit ($\epsilon = 0.4$)

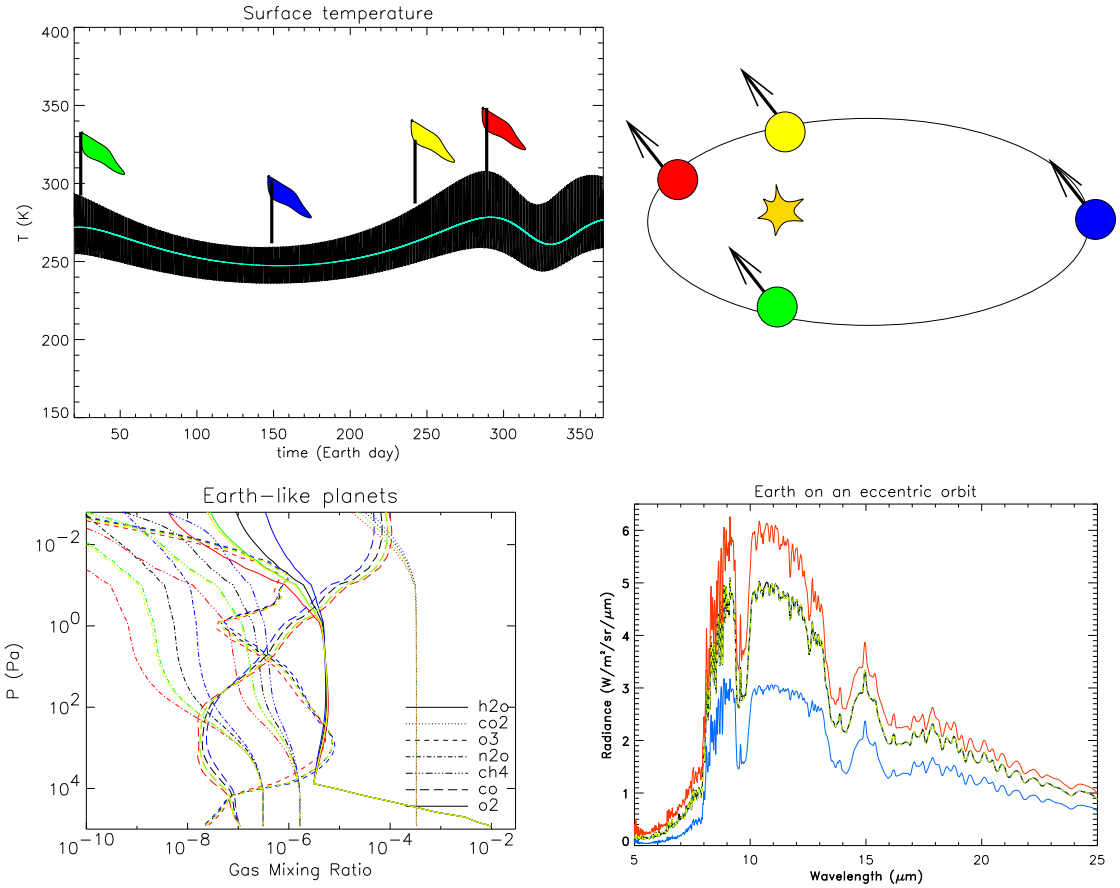

Figure 16: *Earth on a eccentric orbit [ref. 9, 10] is a product of the combination of a chemistry/climate/radiative transfer models. The different colors correspond to different orbital positions (fig. on the top, right). The preliminary results are sensible: the closer is the planet to the star the more some elements like N_2O, H_2O and methan are depleted in the upper atmosphere by photolysis. Unfortunately these elements are hardly detectable in the spectra, due to the strong absorption of H_2O in the same bands, so the main differences in the spectra are due to the changed temperature profiles.*

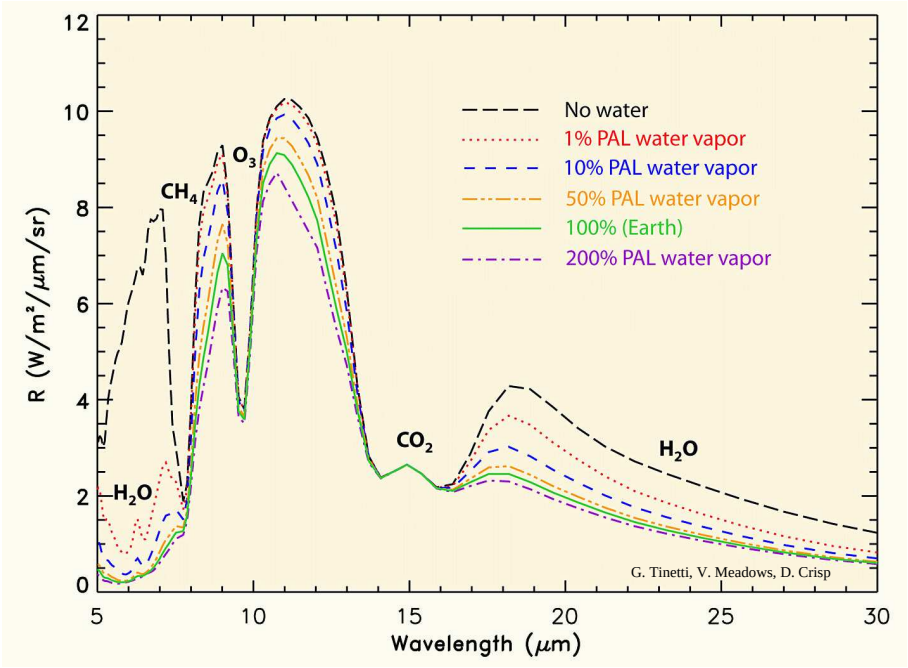

Figure 17: *Synthetic spectra (low resolution ~ 20) of Earth-like planets with different atmospheric water vapor abundances (given as % of Present Atmospheric Level, PAL)*

Conclusions

- Our approach is feasible. The comparison with the experiment confirms: the model works (see fig. 10, 11)!
- We can distinguish among different surface types looking at the Earth's spectra in the visible (0.7-0.8 μm band, red-edge), there are almost no differences in the IR (fig. 5).
- The contribution of clouds is dramatic. We have to include them in order to have a realistic model (fig. 6, 10, 9)
- The temperature inversion in the Earth's atmosphere, which produces the emission peak at the center of the CO_2 15μm band, can be used as a secondary (confirmation) indicator of the presence of a high-altitude absorber such as ozone.
- Although it is possible to discriminate between Mars and Earth at R~20, at higher resolution we are much better able to characterize the temperatures of the surface and atmosphere via features such as the CO_2 15μm band (fig. 12, 14).
- The lack of high spectral resolution smears out the spectral features. However some of the strongest features are detectable with TPF (fig. 12, 13, 14, 15, 17).

- Time dependent variations in the disk-averaged spectra, or "light-curve" can provide additional information about spatial variations (fig. 8, 9, 7).
- The red-edge biosignature is easily detectable when we consider a cloud-free Earth. If clouds are randomly distributed and in high %, it is very hard to detect this signal (fig. 9).
- Earth on a eccentric orbit is a product of the combination of a chemistry/climate/radiative transfer models. The results are sensible. No experiment for the moment to confirm these completely synthetic spectra (fig. 16). Waiting for TPF/Darwin ...

References

.

[Ref. 1] *Initial data from the Mars Global Surveyor thermal emission spectrometer experiment: Observations of the Earth*, P. R. Christensen, J. C. Pearl, Journal of Geophysical research Vol. 102, May 25, 1997

[Ref. 2] V. S. Meadows, D. Crisp, *Ground-based near-infrared observations of the Venus night-side: The thermal structure and water abundance near the surface*, (Journal of Geophysical Research, vol. 101, 4595-4622)

[Ref. 3] Crisp D., *Absorption of sunlight by water vapor in cloudy conditions: A partial explanation for the cloud absorption anomaly.* , Geophys. Res. Lett., 24, 571-574, 1997.

[Ref. 4] Healpix (Hierarchical Equal Area and iso-Latitude Pixelisation) is a curvilinear partition of the sphere into exactly equal area quadrilaterals of varying shape. Healpix was originally designed for the ESA Planck and NASA WMAP (Wilkinson Microwave Anisotropy Probe) missions by Krzysztof M. Górski, Eric Hivon, Benjamin D. Wandelt, (1998).
http://www.eso.org/science/healpix/index.html

[Ref. 5] C.A. Beichman, N. J. Woolf, and C.A. Lindensmith, Eds. *The Terrestrial Planet Finder*, (JPL: Pasadena), JPL 99-3,1999.

[Ref. 6] C.A. Beichman, and T. Velusamy, "Sensitivity of TPF Interferometer for Planet Detection", *Optical and IR Interferometry from Ground and Space.* S.C.Unwin, and R.V. Stachnick, eds. ASP Conference Series, Vol.194 (San Francisco: ASP), 405, 1999.

[Ref. 7] E. Fishbein, C.B. Farmer, S.L. Granger, D.T. Gregorich, M.R. Gunson, S.E. Hannon, M.D. Hofstadter, S.-Y. Lee, S.S Leroy; *Formulation and Validation of Simulated Data for the Atmospheric Infrared Sounder (AIRS)*, IEEE TRANSACTIONS ON GEOSCIENCE & REMOTE SENSING, Vol. 41, N. 2, Feb 2003 1.

[Ref. 8] G. Tinetti, V. S. Meadows, D. Crisp, W. Fong, T. Velusamy, H. Snively; *Disk-averaged synthetic spectra of Mars*, submitted to Astrobiology, 2004.
http://arxiv.org/abs/astro-ph/0408372

[Ref. 9] G. Tinetti, V. S. Meadows, D. Crisp, M. Allen; *Sensitivity of extrasolar terrestrial planets' climate to different orbital geometries*, Astrobiology vol. 4, n. 2, 2004

[Ref. 10] L. Sertorio and G. Tinetti; *Constraints in the coupling star-life*, "il Nuovo Cimento", vol. 25 C, n. 4, 2002

[Ref. 11] R. A. Hanel, B. J. Conrath, D. E. Jennings, R. E. Samuelson, *Exploration of the Solar System by Infrared Remote Sensing*, Cambridge Planetary Science Series 7, 1992

[Ref. 12] Arnold L., Gillet S., Lardire O., Riaud P., Schneider J.: 2002, "A test for the search for life on extrasolar planets: Looking for the terrestrial vegetation signature in the Earthshine spectrum" Astronomy and Astrophysics, 392, 231

This work has been supported by NASA Astrobiology Institute and National Academies.